Inorganic Chemistry

pubs.acs.org/IC
Article

Supramolecular Assembly of Chiral Lanthanide Triple-Decker Metallocyclophanes $Ln_3(L^{meta})_3(L^{R/S})_3$ or Tetrahedral Cages $Ln_4(L^{para})_4(L^{R/S})_4$ and Their Chiroptical Properties

Chi-Tung Yeung, Sai-Kit Cheung, Ho-Yin Wong, Wesley Ting Kwok Chan, Junhui Zhang, Chun-Ming Chan, Wai-Lun Man, and Ga-Lai Law*

Cite This: *Inorg. Chem.* 2025, 64, 20927−20938

Read Online

ACCESS | Metrics & More | Article Recommendations | Supporting Information

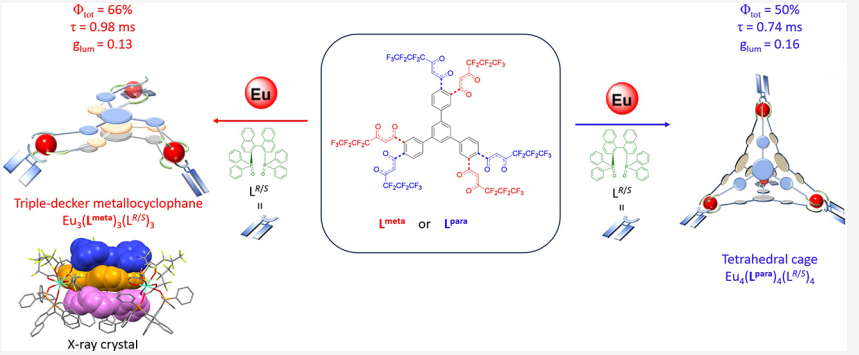

ABSTRACT: Two new ligands (L^{meta}: *meta*-tris-β-diketonate and L^{para}: *para*-tris-β-diketonate) with meta and para orientations of coordinating bidentate β-diketonate units were synthesized in order to investigate their supramolecular formation behavior. When chiral (*R*)- or (*S*)-BINAPO ($L^{R/S}$) was used as a chiral inducer, trinuclear triple-decker metallocyclophane, $Eu_3(L^{meta})_3(L^{R/S})_3$, was formed from L^{meta}, whereas a tetranuclear tetrahedral cage $Eu_4(L^{para})_4(L^{R/S})_4$ was formed with L^{para}. The X-ray crystal of $Eu_3(L^{meta})_3(L^{S})_3$ shows that all three Eu centers possess the same configuration, hence resulting in homochiral ΔΔΔ assembly. The triple-decker exhibited a longer luminescence lifetime (∼0.98 ms vs ∼0.74 ms) and higher quantum yields (∼66% vs ∼50%) than the tetrahedral cage. Moreover, chiroptical properties were observed for a lanthanide triple-decker metallocyclophane: Mirror-image circular dichroism of chiral $Eu_3(L^{meta})_3(L^{R/S})_3$ or $Eu_4(L^{para})_4(L^{R/S})_4$ discloses their enantiomeric behavior and chiral transmission from (*R*)- or (*S*)-BINAPO moiety to achiral L^{meta} and L^{para}. Furthermore, their circularly polarized luminescence indicated that the $|g_{lum}|$ can reach 0.13 for the triple-decker metallocyclophane and 0.16 for the tetrahedral cage.

INTRODUCTION

Development of circularly polarized luminescence (CPL) materials is a continuous, expanding research topic in recent years due to its potential applications in different areas such as molecular probes,[1] three-dimensional displays,[2] molecular photoswitches,[3,4] optical storage,[5] and advanced medical imaging.[6] Due to their advantageous magnetic dipole character, lanthanides are generally regarded as favorable candidates in many CPL studies.[7−18] Their superior high luminescence dissymmetry factor (g_{lum} = 1−10^{-2}), which are in general 500−1000 times higher than organic luminophores (g_{lum} = 10^{-3}−10^{-5})[19−21] allows for more feasible applications in the real world. To the best of our knowledge, complexes with top reported $|g_{lum}|$ values in solution are all based on chiral β-diketone tetrakis(camphorate) Eu(III) unit.[22] Recently, an improved $|g_{lum}|$ of up to 1.54 was reported, along with a higher quantum yield, from $TEA^+[Eu[(+)\text{-tfc}]_4]^-$ complex (TEA = tetraethylammonium, (+)-tfc = (+)-3-trifluoroacetylcamphorate).[23] So the search and development of new, innovative, and robust materials with high quantum yields and g_{lum} values is still one of the major tasks in the development of CPL-active materials.

Coordination-driven self-assembly is known to be one of the effective/powerful methods to synthesize discrete, nanoscale supramolecular architectures.[24−32] In the past decades, there have been exhaustive examples of fascinating transition metal-based supramolecules where some of them have demonstrated diverse applications such as behaving as reaction vessels or catalysts,[33−36] used for host/guest encapsulation,[37,38] a drug

Received: June 3, 2025
Revised: July 25, 2025
Accepted: August 5, 2025
Published: August 19, 2025

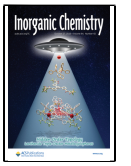

https://doi.org/10.1021/acs.inorgchem.5c02534
Inorg. Chem. 2025, 64, 20927−20938

Scheme 1. Self-Assembly of Triple-Decker Metallocyclophane $Ln_3(L^{meta})_3(L^{R/S})_3$ and Tetrahedral Cage $Ln_4(L^{para})_4(L^{R/S})_4$ from L^{meta} and L^{para} Ligands

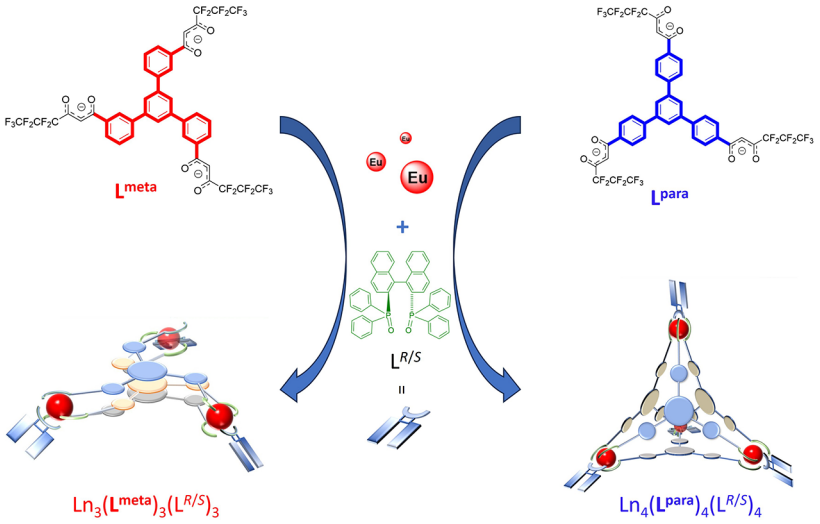

delivery transporter,[39−41] or as molecular recognition and separation tools.[42,43] On the contrary, high order topology of lanthanide supramolecules is relatively less developed.[44−50] This may be attributed to the innate lanthanide coordination kinetic lability and coordination number variety that make the prediction of the resulting supramolecular structures difficult. The preparation of chiral assemblies, coordination dynamics, and orderless stereoselective selection of lanthanide ions makes it possible to successfully obtain stereospecific supramolecular assemblies. In recent years, a number of impressive chiral lanthanide supramolecular assemblies, including helix,[51−69] tetrahedron,[70−80] cubes,[81,82] and other multinuclear assemblies,[53,64,83−86] which were based on rational chiral ligand design and strategic control of a lanthanide ion to ligand ratio, were reported. On some occasions, CPL activities were observed from some of these examples.[10,11,51−54,57−59,61,63,64,70−72,74,77,78,83,85] Among them, one of the assemblies, an octanuclear circular helicate [(*R*)- or (*S*)-^{i}Pr-Pybox]$_8$(Eu^{III})$_8$(THP)$_8$ (THP = trianionic tris-*β*-diketonate), exhibited extraordinary CPL activity ($|g_{lum}|$ up to 1.25).[64] Together with its 14.5% luminescent quantum yield, the difference in CPL intensity, which is observed by the naked eye, from the corresponding *R* and *S* isomers, was reported for the first time.

For the sake of simplicity, the majority of reported chiral lanthanide supramolecular assemblies can be generally classified as a (one plus one)/two-component composition, which contains one type of ligand and one type of lanthanide ion in coordination geometry.[55,56,58,63,72−74,77,78] Due to randomness, the synthesis of (two plus one)/three-component assemblies with two types of ligands (L′ and L″) and one type of metal ion is more complicated. Even if the two ligand-to-metal ratio is accurately and carefully controlled, successful formation of chiral supramolecular assemblies is not guaranteed. In the last eight years, a number of fascinating examples of three-component assemblies based on (a) bis- or tris-*β*-diketonate ligands as the first component, (b) achiral or chiral ligands as the second component, and (c) lanthanide as the third component appeared. Apart from common assemblies such as helixes,[51] tetrahedral cages,[70,71] and other uncommon multinuclear species such as octanuclear[64] or tetranuclear[53,83] circular helicates from these three-component assemblies were observed. Intense CPL ($|g_{lum}|$ = up to 1.25) was observed for some of the cases. These satisfactory results allow us to rationally design two new tris-*β*-diketonate ligands, HL^{para} and HL^{meta}, to develop new and novel chiral supramolecular assemblies (Scheme 1). Their potential to be developed as CPL material will be investigated as well. To the best of our knowledge, our triple-decker is the first chiral lanthanide triple-decker metallocyclophane to be reported with concrete potential to be applied as a CPL material.

RESULTS AND DISCUSSION

Ligand Design and Synthesis. Supramolecular self-assembly is highly sensitive to the variations of ligand geometry. Even with a slight change in ligand bend angles, a vast difference in the final supramolecular structures would be observed.[87] For lanthanide assemblies, investigation of the effect of ligand geometry on supramolecular assemblies is rather limited but important.[88−91] When the bend angle between a linker and a tridentate coordination unit was varied from 180° to 120° degrees, the corresponding 9-coordinated lanthanide assemblies were observed to be tetrahedra and sandwich structures, respectively.[89] This interesting difference in supramolecular structure persuaded us to apply a similar bend angle changing strategy on the tris-*β*-diketonate ligand. This difference is expected to induce different chiroptical properties in the resulting lanthanide supramolecular assemblies, which are previously rather limited or less disclosed. Herein, HL^{meta} and HL^{para} with two slightly different topologies were developed. The two tripodal ligands, HL^{meta} and HL^{para}, were synthesized in two steps. The first step involved Suzuki coupling of 1,3,5-tribromobenzene with either 3-acetyl or 4-acetylphenyl boronic acid to afford the corresponding meta- or *para*-triacetyl-triphenyl benzene intermediate S1 and S2 (Figures S1−S10 in Supporting Information). The second step was a modified Claisen condensation reaction of S1 or S2 with ethyl heptafluorobutrate to obtain the HL^{meta} and HL^{para}.

Complex of Triple-Decker Metallocyclophane $Eu_3(L^{meta})_3(L^{R/S})_3$ when $L^{R/S}$ = (*R*)-/(*S*)-BINAPO as Ancillary Ligand. Originally, HL^{meta} and HL^{para} with different spanning

https://doi.org/10.1021/acs.inorgchem.5c02534
Inorg. Chem. 2025, 64, 20927−20938

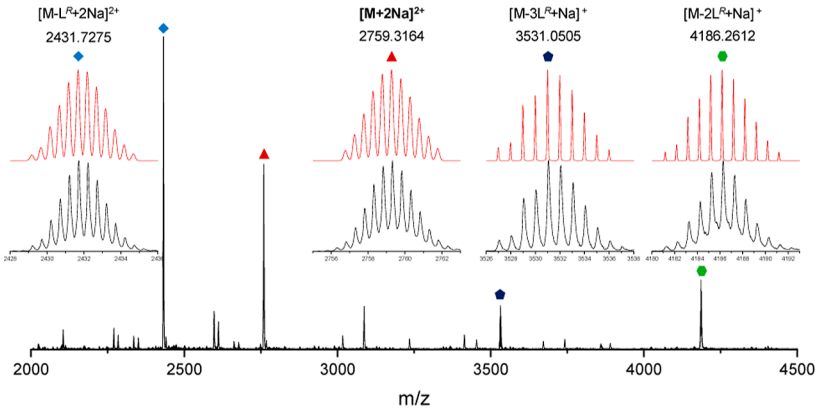

Figure 1. ESI-MS of triple-decker metallocyclophane $Eu_3(\mathbf{L}^{meta})_3(L^R)_3$. Inset showing the isotopic patterns (upper-red) and experimental (lower-black) isotopic patterns.

angles (120° vs 180°) were expected to form tetrahedral cages with different sizes of internal cavity. However, they were finally found to form very different supramolecular assemblies, as $\mathbf{HL}^{meta}$ formed a triple-decker metallocyclophane, whereas $\mathbf{HL}^{para}$ formed a tetrahedral cage. The triple-decker metallocyclophane, $Eu_3(\mathbf{L}^{meta})_3(L^{R/S})_3$, was synthesized by using a one-pot subcomponents synthetic strategy by reacting equimolar amounts of triethylamine-treated-$\mathbf{HL}^{meta}$, (*R*)/(*S*)-BINAPO and $EuCl_3$ in a mixture of MeOH and CH_2Cl_2 at refluxing temperature. Although the triple-decker metallocyclophane is a noncharge carrying species, high resolution mass spectrometry can still be used to support the hypothesis of the triple-decker metallocyclophane species. For instance, there are peaks at *m*/*z* 2579.3164, 2431.7275, 4186.2612, and 3531.0505 corresponding to zero, one, two, and three ancillary ligand(s) ($L^{R/S}$) as $[M + 2Na]^{2+}$, $[M - 1L^{R/S} + 2Na]^{2+}$, $[M - 2L^{R/S} + Na]^{+}$, and $[M - 3L^{R/S} + Na]^{+}$ (Figures 1, S11 and S12) detaching from the parent species of $Eu_3(\mathbf{L}^{meta})_3(L^{R/S})_3$. These assignments were further supported when their isotopic distributions of the calculated and experimental results were compared.

A series of NMR experiments were then utilized to understand the complex formation of this species (Figures S13−S23). The ^{1}H NMR spectrum of the triple-decker $Eu_3(\mathbf{L}^{meta})_3(L^{R/S})_3$ shows a highly convoluted peak pattern spread from a wide chemical shift range with paramagnetic peak broadening, and no reasonable assignments can be made (Figures S13 and S14). However, a clearer picture was available from ^{19}F and ^{31}P NMR. These NMR experiments can be utilized to probe the symmetry of the triple-decker structure by the ligand subcomponents. From the ^{19}F NMR, the arrangement of the $\mathbf{L}^{meta}$ ligand can be determined as C_3-symmetric. Chemical shift of ligand CF_3 (−80.47 ppm) was split into three peaks (I: −80.11 ppm; II: −80.39 ppm, III: −83.26 ppm) with 1:1:1 intensity (Figures 2a, S15, and S16). The ^{31}P NMR from the $L^{R/S}$ ligand shows strong upfield-shifted peaks from a single peak of +28 ppm to two peaks at −43 and −48 ppm after coordination, revealing the inequivalence of the two phosphorus atoms in the $L^{R/S}$ ligand (Figures 2b, S17, and S18). Therefore, no C_2-symmetric axis was observed from $L^{R/S}$, indicating the overall C_3-symmetrical structure by coordination self-assembly. Further information from the ^{1}H diffusion-ordered NMR spectroscopy (DOSY) showed peaks corresponding to the assembly in a single band at a diffusion coefficient of $D = 2.61 \times 10^{-10}$ m^2 s^{-1}, supporting

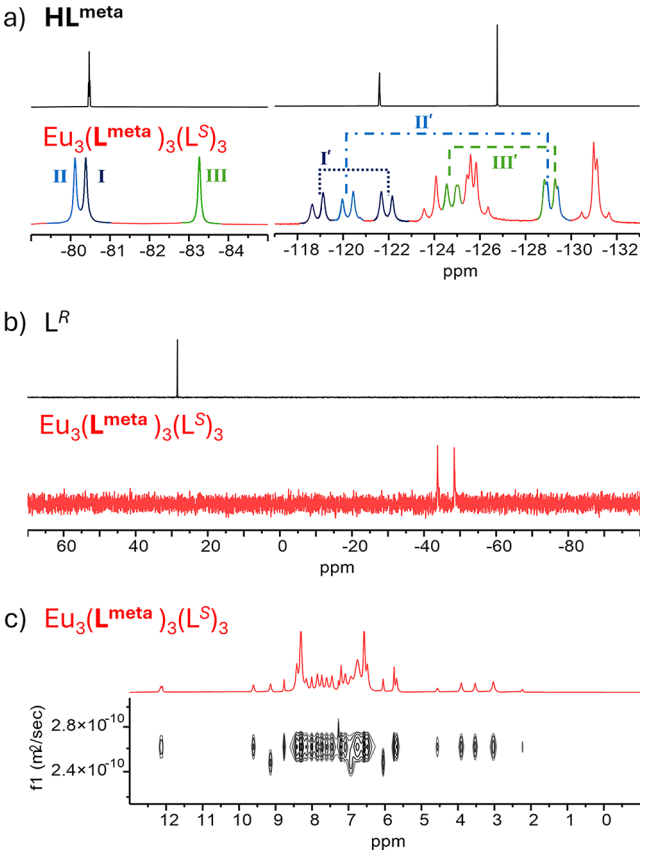

Figure 2. (a) ^{19}F NMR of $\mathbf{HL}^{meta}$ (upper) and $Eu_3(\mathbf{L}^{meta})_3(L^S)_3$ (lower) (correlation: −80.11(II)∩−119.97, −120.44, −128.83, −129.29; −80.39(I)∩−118.65, −119.13, −121.68, −122.16; −83.26-(III)∩−124.54, −125.00, −128.93, and −129.41). ($CDCl_3$, 293 K). (b) ^{31}P NMR of (*S*)-BINAPO (upper) and $Eu_3(\mathbf{L}^{meta})_3(L^S)_3$ (lower). ($CDCl_3$, 293 K). (c) ^{1}H DOSY NMR of $Eu_3(\mathbf{L}^{meta})_3(L^S)_3$. ($CDCl_3$, 293 K).

the formation of a single species (Figures 2c, and S19). Then, 2D ^{19}F−^{19}F COSY NMR was employed to assign the ^{19}F NMR peaks: three vicinal CF_3−CF_2* coupling pairs (I∩I′; II∩II′; III∩III′) are observed in the cross peak at the −75 to −135 ppm region (Figures 2a, and S20). The residual peaks from the COSY spectra can be assigned to the inner CF_2 unit. Through these triple splitting patterns of ^{19}F NMR chemical shifts ($-CF_3$), three layers of C_3F_7 chains can be hypothesized

https://doi.org/10.1021/acs.inorgchem.5c02534
Inorg. Chem. 2025, 64, 20927−20938

to indicate a C_3-symmetrical structure. ^{1}H−^{1}H COSY spectra were used to indicate the corresponding singlet uncoupled protons; parts of these identified singlet protons can be assigned by the correlation from the ^{1}H−^{1}H NOESY NMR (Figures S21−S23).

X-ray Crystal Structure of Triple-Decker Metallocyclophane $Eu_3(L^{meta})_3[L^S]_3$. The crystals of $Eu_3(L^{meta})_3[L^S]_3$ were grown by slow diffusion of methyl *tert*-butyl ether into a dichloromethane solution of the complex. The structure was confirmed by X-ray single crystal analysis; it crystallizes in the monoclinic space group $P2_1$. It consists of three 8-coordinated Eu centers bearing a distorted square antiprism geometry (average Eu···O distance = 2.393 Å, ∠O···Eu···O = 75.39°) (Figure 3). The vertices of one base are rotated between 42° to 49° relative to the other, deviating from the angle of 45° in an ideal square antiprism geometry. The bulkiness of the (*S*)-BINAPO ligand has exerted its influence on the coordination environment and is the reason for the obvious distortion from ideal square antiprism geometry.

The triangular arrangement of the Eu centers (average Eu··· Eu distance = 12.991 Å) mirrors the arrangement of the *β*-diketone moieties that radiate from the center of the ligand L^{meta}, in which a general C_3-symmetry is inherited from the ligand itself. The three L^{meta} ligands are observed to be in a triple-decker, sandwich-like arrangement, wherein relatively strong $\pi-\pi$ interactions arise from the near-perfect overlapping of the central phenyl rings (average interplanar distance = 3.459 Å). In order to induce a suitable coordination environment that is affected by the bulky (*S*)-BINAPO ligands, rotations took place between the phenyl−phenyl planes and the phenyl−diketonate planes, generating a helical, twisted propeller-like conformation as a result. Such rotations are more notable within the top and the bottom L^{meta} layers, in which angles between planes exceed 30°. More interestingly, the top and bottom layers rotated in opposite directions, leading to one anticlockwise and one clockwise propeller structure. While the middle layer also carries an anticlockwise conformation, the opposing rotations still allow a ΔΔΔ configuration to be observed at the three Eu centers. A second implication is that further $\pi-\pi$ interactions are rendered impossible, as phenyl rings have rotated away from conditions suitable for face-to-face interactions, but not enough to allow edge-to-face interactions. Although interactions between layers of L^{meta} are restricted to the central $\pi-\pi$ interactions, weaker interactions in the form of CH−π interactions and hydrogen bonding with the fluoroalkyl chains are available between L^{meta} and (*S*)-BINAPO, helping to stabilize the overall structure. Unfortunately, the fluoroalkyl chains are heavily disordered, and thus the extent of their interactions with (*S*)-BINAPO cannot be ascertained. This is similarly the case with solvent molecules. Existing in the lattice is a large void with a calculated volume of 6045.3 Å^3, occupying 37.5% of the total unit cell volume (16126 Å^3). The extremely diffuse residue electron density made identification of the lattice solvent impractical.

Complex of Tetrahedral Cage $Eu_4(L^{para})_4(L^{R/S})_4$ when $L^{R/S}$ = (*R*)-/(*S*)-BINAPO as Ancillary Ligand. Different from forming the triple-decker metallocyclophane with L^{meta}, our original proposed tetrahedral cage formation was successfully obtained when L^{para} was used as a ligand. The synthesis of $Eu_4(L^{para})_4(L^{R/S})_4$ was similar to the previous triple-decker metallocyclophane. After reacting equimolar amounts of triethylamine-treated-HL^{para}, (*R*)/(*S*)-BINAPO, and $EuCl_3$ in

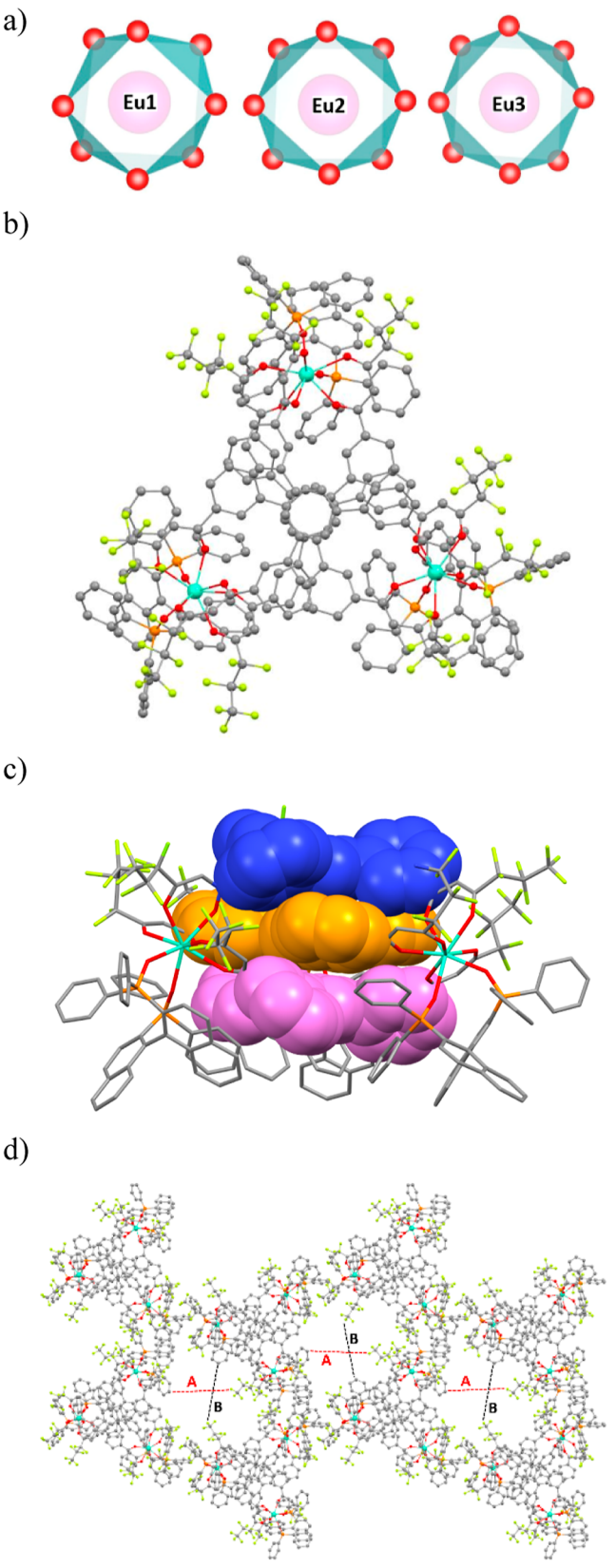

Figure 3. (a) Coordination polyhedron surrounding the Eu Centres. (b) Top-down view of the complex $Eu_3(L^{meta})_3(L^S)_3$. (c) Side view of $Eu_3(L^{meta})_3(L^S)_3$. The phenyl rings of L^{meta} are shown in space-filling to show their stacking arrangement. The opposite rotation of the top and bottom L^{meta} layers can be seen clearly. (d) Packing diagram viewed down the *a*-axis. The very large solvent accessible void is clearly visible (red dots A = 11.47 Å; black dots B = 10.86 Å).

https://doi.org/10.1021/acs.inorgchem.5c02534
Inorg. Chem. 2025, 64, 20927−20938

a mixture of MeOH and CH_2Cl_2 at refluxing temperature. Successful formation of these tetranuclear species was confirmed with high-resolution ESI-TOF-MS. A series of peaks corresponding to $Eu_4(\mathbf{L}^{para})_4(L^{R/S})_{4-n}$ (n = 0 to 4) with m/z of 3671.3433, 3433.7822, 3016.6682, 2689.0686, and 2361.9514 correspond to the sequential loss of $L^{R/S}$ ancillary ligand(s) [$[M + 2Na]^{2+}$, $[M-1L^{R/S} + 2Na]^{2+}$, $[M - 2L^{R/S} + 2Na]^{2+}$, $[M - 3L^{R/S} + 2Na]^{2+}$, and $[M - 4L^{R/S} + 2Na]^{2+}$ (Figures S24, and S25)] from of the intact tetranuclear structure $Eu_4(\mathbf{L}^{para})_4(L^{R/S})_4$ as. The isotopic pattern further confirms the formation of the species.

The ^{1}H NMR spectrum of the $Eu_4(\mathbf{L}^{para})_4(L^{R/S})_4$ shows a more overlapping chemical shift than the triple-decker metallocyclophanes (Figures S26 and S27). Moreover, the splitting patterns in ^{19}F NMR and ^{31}P NMR are different from the triple-decker metallocyclophanes. For ^{19}F NMR, only three ^{19}F chemical shifts for the $-CF_2CF_2CF_3$ unit appeared, which indicates a high symmetry of the $Eu_4(\mathbf{L}^{para})_4(L^{R/S})_4$ (Figures S28, and S29). Interestingly, only one chemical shift was observed in the ^{31}P NMR to indicate the C_2 symmetry nature of the chiral BINAPO is intact in the complex (Figures S30, and S31). Further information from the DOSY showed a single band at a diffusion coefficient of $D = 2.44 \times 10^{-10}$ m^2 s^{-1}, supporting the formation of a single species (Figure S32).

Photophysical Properties. The UV−vis absorption and photoluminescent properties of the complexes, $Eu_3(\mathbf{L}^{meta})_3(L^{R/S})_3$ and $Eu_4(\mathbf{L}^{para})_4(L^{R/S})_4$, were studied in acetonitrile. $\mathbf{L}^{meta}$ and $\mathbf{L}^{para}$ show bands originating from intraligand charge transfer (ILCT) transition from phenyl rings to the β-diketonate moieties shift hypochromically when the corresponding complexes were compared ($\mathbf{L}^{meta}$: λ_{max} from 321 to 330 nm and $\mathbf{L}^{para}$: λ_{max} from 332 to 357 nm) (Figure 4a). These extensive shifts can be realized by electron conjugation disruption by conformational twisting between the phenyl rings and β-diketonate moieties when the complexes were formed.

The excitation and emission of the two assemblies, $Eu_3(\mathbf{L}^{meta})_3(L^{R/S})_3$ and $Eu_4(\mathbf{L}^{para})_4(L^{R/S})_4$, were studied (Table 1, Figures S33 and S44). The excitation bands and absorption bands in the region of 290−400 nm are well matched to each other. Upon excitation at 350 nm, characteristic emission bands at 580, 594, 613, 650, and 702 nm of Eu(III) ions arising from the $^5D_0 \rightarrow {}^7F_J$ (J = 0−4) transitions were observed (Figure 4b). Both of the assemblies have an intense electric dipole hypersensitive $^5D_0 \rightarrow {}^7F_2$ transition. High-resolution emission spectra of $Eu_3(\mathbf{L}^{meta})_3(L^{R/S})_3$ and $Eu_4(\mathbf{L}^{para})_4(L^{R/S})_4$ at 77 K were recorded to probe their structures in the solution state and to study the site symmetry via the splitting patterns of the different corresponding transitions (Figures S45 and S46). For both assemblies, the crystal field splitting in the $^5D_0 \rightarrow {}^7F_1$ transition resulted in three peaks, suggesting a low symmetry environment for these Eu(III) ions.[92−94] The splitting patterns at other energy levels in these two Eu(III) compounds are also similar, indicating that the Eu(III) ions should share a similar coordination environment. In addition, lifetime measurements were performed to confirm the stability of the $Eu_3(\mathbf{L}^{meta})_3(L^{R/S})_3$ and $Eu_4(\mathbf{L}^{para})_4(L^{R/S})_4$, where no notable changes in lifetime were observed upon dilution.

Since the quantum yields for the two assemblies are different ($Eu_3(\mathbf{L}^{meta})_3(L^{R/S})_3$: ∼66% and $Eu_4(\mathbf{L}^{para})_4(L^{R/S})_4$: ∼50%), they indicate that the sensitization efficiency of $\mathbf{L}^{meta}$ and $\mathbf{L}^{para}$ in the corresponding complexes is different as well. The $\pi-\pi$ stacking conformation in the triple-decker metallocyclophane may enhance efficient energy transfer and result in higher quantum yield, but no such phenomenon exists for the tetrahedral cage. To further study the energy transfer pathway of $Eu_3(\mathbf{L}^{meta})_3(L^{R/S})_3$ and $Eu_4(\mathbf{L}^{para})_4(L^{R/S})_4$, Gd^{3+} analogues were synthesized and low temperature measurements were conducted at 77 K in the glassy mixture of EtOH/MeOH = 4:1 (Figures S47−S56). The phosphorescence spectra of $Gd_3(\mathbf{L}^{meta})_3(L^S)_3$ and $Gd_4(\mathbf{L}^{para})_4(L^S)_4$ were then recorded due to the presence of heavy atom effects from Gd^{3+}, and the reduction in nonradiative decay under a low-temperature environment. The phosphorescence obtained was further confirmed through lifetime measurements at 77 K, which showed the typical phosphorescence time range in milliseconds. Hence, the triplet states of these two supramolecular systems could be revealed, and the corresponding Jablonski diagrams were plotted (Figures S57, and S58). The triplet states in the range around 21322 cm^{-1} and 20408 cm^{-1} were calculated for $Gd_3(\mathbf{L}^{meta})_3(L^{R/S})_3$ and $Gd_4(\mathbf{L}^{para})_4(L^{R/S})_4$, respectively, for ligand $\mathbf{L}$ and BINAPO (^{1}T = 19841 cm^{-1}).[95,96] According to the $\lambda_{Em,max}$ in their phosphorescence spectra, the energy differences are 4058 cm^{-1} and 3144 cm^{-1}

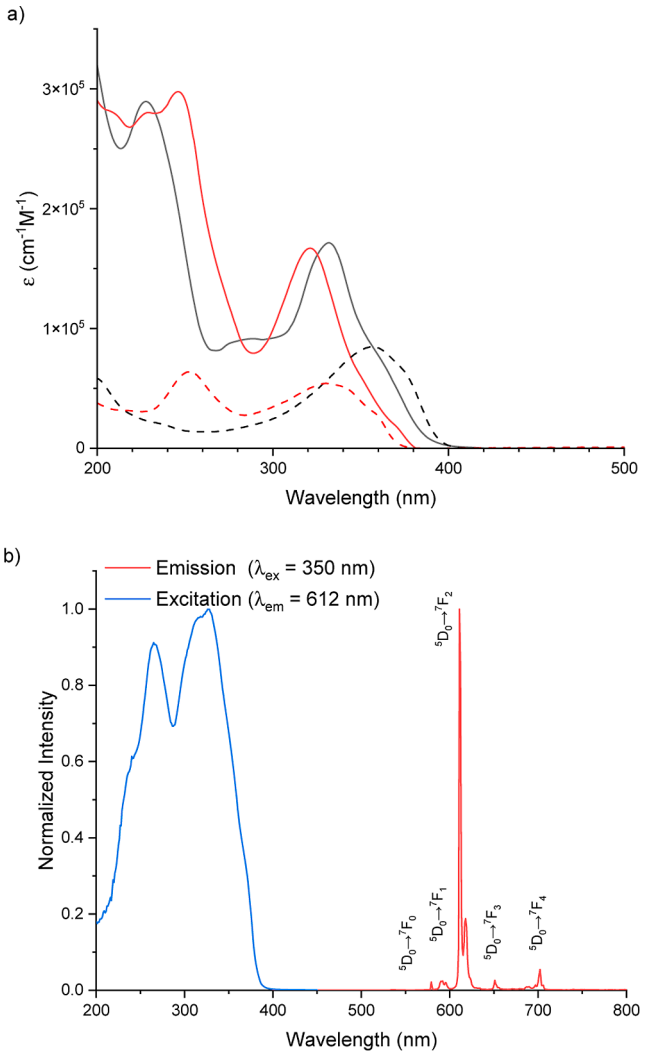

Figure 4. (a) UV−vis spectra of $\mathbf{L}^{meta}$ (Red, dashed line), $\mathbf{L}^{para}$ (Black, dashed line), $Eu_3(\mathbf{L}^{meta})_3(L^{R/S})_3$ (Red, solid line), and $Eu_4(\mathbf{L}^{para})_4(L^{R/S})_4$ (Black, solid line). (b) Photoluminescence spectra of $Eu_3(\mathbf{L}^{meta})_3(L^R)_3$ in acetonitrile.

https://doi.org/10.1021/acs.inorgchem.5c02534
Inorg. Chem. 2025, 64, 20927−20938

Table 1. Photophysical Measurements of $Eu_3(L^{meta})_3(L^{R/S})_3$ and $Eu_4(L^{para})_4(L^{R/S})_4$[a,d]

complexes	UV λ_{max} (nm)	$Ex_{\lambda max}$ (nm)	Φ_{tot} (%)[b]	Φ_{Eu}^{Eu} (%)[c]	τ (ms)	η_{sens}[c]	g_{lum} ($^5D_0 \rightarrow {}^7F_1$)	g_{lum} ($^5D_0 \rightarrow {}^7F_2$)
$Eu_3(L^{meta})_3(L^S)_3$	322	325	66.1	72.6	0.980	0.91	+0.13	−0.01
$Eu_3(L^{meta})_3(L^R)_3$	321	326	66.4	71.2	0.971	0.93	−0.13	+0.01
$Eu_4(L^{para})_4(L^S)_4$	332	332	50.0	62.1	0.736	0.81	+0.16	−0.01
$Eu_4(L^{para})_4(L^R)_4$	332	331	50.7	61.8	0.739	0.82	−0.16	+0.01

[a]All of the measurements were conducted in spectroscopic grade acetonitrile. [b]Quantum yields were measured with 370 nm (excitation) using a calibrated integrating sphere and calculated to be within 5% error. [c]See Experimental section for details. [d]UV-vis absorption maximum (λ_{max}), excitation maximum ($Ex_{\lambda max}$), overall quantum yield (Φ_{tot}), intrinsic quantum yield (Φ_{Eu}^{Eu}), emission lifetime of Eu(III) (τ), sensitization efficiency (η_{sens}), and g_{lum}.

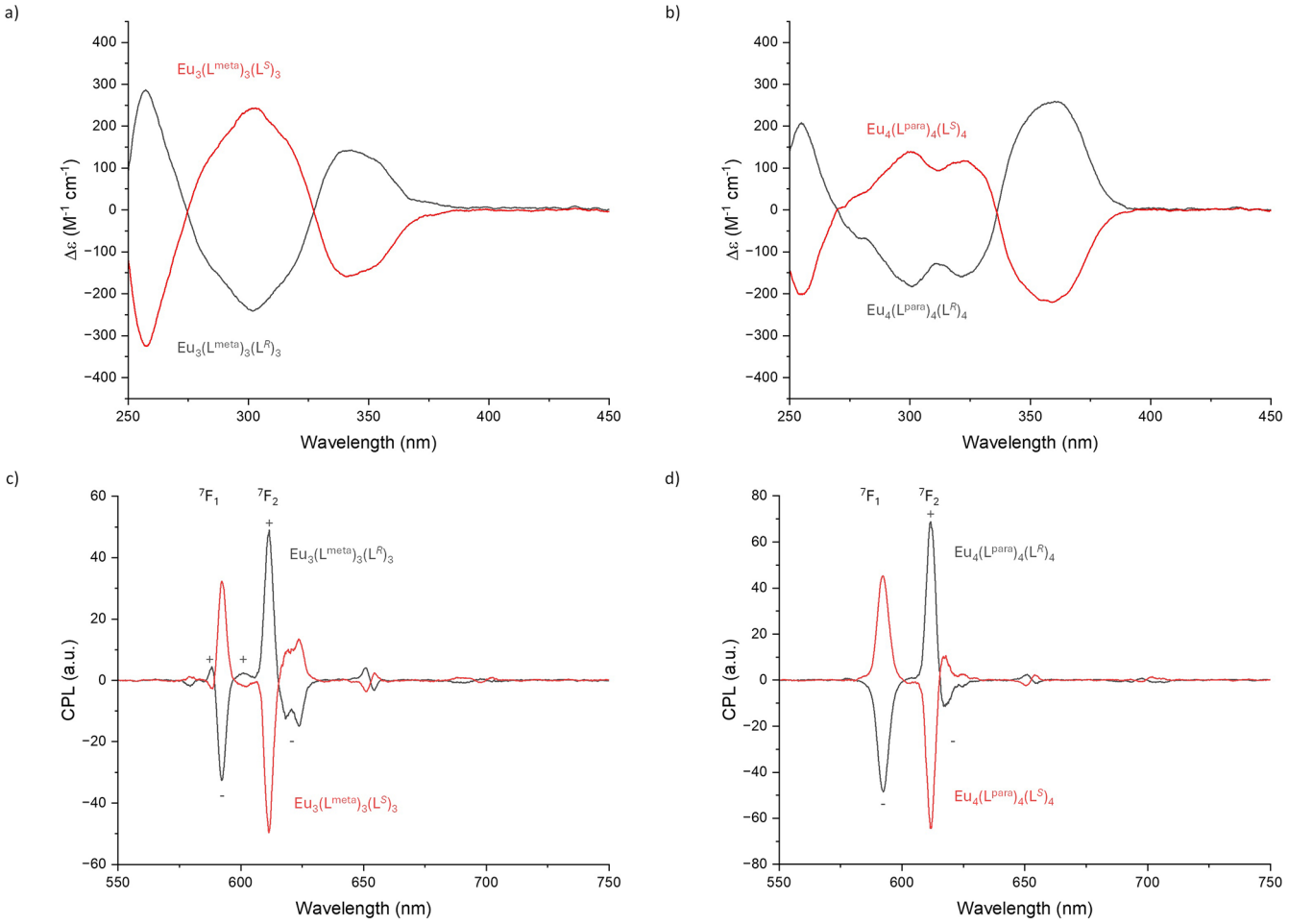

Figure 5. CD spectra of enantiomeric pairs of (a) $Eu_3(L^{meta})_3(L^R)_3$ and $Eu_3(L^{meta})_3(L^S)_3$ and (b) $Eu_4(L^{para})_4(L^R)_4$ and $Eu_4(L^{para})_4(L^S)_4$. CPL spectra of enantiomeric pairs of (c) $Eu_3(L^{meta})_3(L^R)_3$ and $Eu_3(L^{meta})_3(L^S)_3$ and (d) $Eu_4(L^{para})_4(L^R)_4$ and $Eu_4(L^{para})_4(L^S)_4$. All of the measurements were performed with acetonitrile in 1×10^{-6} M.

higher than the lowest energy accepting level ($^5D_0$) of Eu^{3+} ion, which both lie within the ideal energy gap (2500−5000 cm^{-1}) for effective energy transfer of lanthanide.[97−100] Within the ideal energy gap, the situations of back energy transfer from lanthanide to ligand or lack of energy transfer from ligand to lanthanide were both avoided, ensuring the effective energy transfer to the lanthanide metal center. This results in high sensitization efficiency (>80%) and high quantum yields (>50%) for $Eu_3(L^{meta})_3(L^{R/S})_3$ and $Eu_4(L^{para})_4(L^{R/S})_4$.

Chiroptical Properties. The *R*- and *S*-assemblies of the corresponding $Eu_3(L^{meta})_3(L^{R/S})_3$ or $Eu_4(L^{para})_4(L^{R/S})_4$ exhibit mirror image CD signals to each other to indicate that they are enantiomers (Figure 5a,b). Since the signal in the 300−400 nm region can be attributed to $\pi-\pi^*$ transition of β-diketonate moieties of the L^{meta} and L^{para} ligands, this induced CD signals that can be considered to originate from induced chiral rotation of the phenyl rings when chiral ancillary ligands (*R*)/(*S*)-BINAPO are coordinated to the Eu(III) ions. This is coherent with the observation of nonplanarity of the phenyl rings from the X-ray structure (Figure 3c). Although both triple-decker metallocyclophane and tetrahedral cages show strong CD signals, the exhibited signals are of different extents. This is attributed to the observable opposing clockwise and anticlockwise propeller conformation from the top and bottom layers of the triple-decker metallocyclophane, also implying that the noncoherent phenyl ring rotation may not happen in the tetrahedral cage.

https://doi.org/10.1021/acs.inorgchem.5c02534
Inorg. Chem. 2025, 64, 20927−20938

Excited state chiroptical properties can be revealed by CPL spectra. $Eu_3(\mathbf{L}^{meta})_3(L^{R/S})_3$ or $Eu_4(\mathbf{L}^{para})_4(L^{R/S})_4$ displayed an almost complete mirroring of CPL profiles to their corresponding *R*- and *S*-isomers. This result implies that their excited state enantiomeric nature is valid (Figure 5c,d). In the $^5D_0 \rightarrow {}^7F_J$ (J = 0−4) transition region, $^5D_0 \rightarrow {}^7F_2$ and $^5D_0 \rightarrow {}^7F_1$ transitions resulted in a more intense CPL signal than other transitions, with $^5D_0 \rightarrow {}^7F_2$ apparently the strongest. Although photoluminescence of the $^5D_0 \rightarrow {}^7F_1$ transitions (595 nm) is weak (Figures S33, S35, S37 and S39), it exhibited a relatively strong CPL intensity. This is due to its characteristic magnetic dipole transition nature, hence fulfilling the magnetic dipole selection rule, $\Delta J = 0, \pm 1$, except 0−0 transition.

When analyzed in detail, the CPL profiles from triple-decker metallocyclophane $Eu_3(\mathbf{L}^{meta})_3(L^{R/S})_3$ and tetrahedral cage $Eu_4(\mathbf{L}^{para})_4(L^{R/S})_4$ possess some distinct feature for differentiation. In the spectra of $Eu_3(\mathbf{L}^{meta})_3(L^{R})_3$ isomer (Figure 5c, black line), the sign of the CPL profile follows the order of (+) and (−) and (+) at $^5D_0 \rightarrow {}^7F_1$ transitions (∼592 nm) and (+) and (−) at $^5D_0 \rightarrow {}^7F_2$ transitions (∼618 nm). Alternatively, for the $Eu_4(\mathbf{L}^{para})_4(L^{R})_4$ isomer (Figure 5d, black line), only (−) was observed at $^5D_0 \rightarrow {}^7F_1$ transitions (∼592 nm) and (+) and (−) at $^5D_0 \rightarrow {}^7F_2$ transitions (∼618 nm) with different signatures were seen. Moreover, their g_{lum} values (Table 1) deviated from each other: Triple-decker $Eu_3(\mathbf{L}^{meta})_3(L^{R/S})_3$ shows $|g_{lum}|$ values of ∼ 0.13 (Figure S59), whereas tetrahedral cage $Eu_4(\mathbf{L}^{para})_4(L^{R/S})_4$ shows ∼0.16 (Figure S60) at the $^5D_0 \rightarrow {}^7F_1$ transition. All this information supports their structural dissimilarity in the solution phase. These levels of $|g_{lum}|$ are comparable to other supramolecular assemblies with similar europium coordination with three *β*-diketonates and one chiral BINAPO, which lie within the usual range of $|g_{lum}|$ values from 0.1 to 0.2.[57,70,71]

CONCLUSIONS

In summary, we successfully synthesized a rare example of chiral lanthanide trinuclear triple-decker metallocyclophane $Eu_3(\mathbf{L}^{meta})_3(L^{R/S})_3$. X-ray crystallography analysis revealed that each 8-coordinated Eu center coordinates to three bidentate *β*-diketonate units and one chiral bidentate phosphine oxide (*S*)-BINAPO to form a distorted square antiprism geometry. The Eu centers in the resulting structures all possess the same ΔΔΔ configuration. In comparison, a tetrahedral cage $Eu_4(\mathbf{L}^{para})_4(L^{R/S})_4$ resulted when $\mathbf{L}^{para}$ was employed. These two different supramolecular assemblies exhibited different photophysical properties such as quantum yields (66 vs 50%), CD (different ellipicity signature), and CPL ($|g_{lum}|$ = 0.13 vs 0.16).

EXPERIMENTAL SECTION

General Information. All solvents and reagents were used as received unless mentioned otherwise. Dry THF is obtained from distillation with calcium hydride. Water-sensitive reactions were carried out under a positive-pressure nitrogen atmosphere. ^1H, ^{13}C, ^{19}F, and ^{31}P NMR spectra were recorded on a Bruker Ultrashield 400 Plus and Bruker Advance-III 600 MHz FT-NMR System. High-resolution mass spectra were obtained on an Agilent 6540 Liquid Chromatography−Electrospray Ionization Quadrupole-Time-of-Flight Mass Spectrometer for organic compounds and Waters Synapt G2-Si High-Definition Ion Mobility Mass Spectrometer for inorganic compounds. For HR-MS of inorganic compounds, soft ionization conditions are used: capillary voltage of 3 kV, sampling cone voltage 40 V, source offset 80 V, source temperature 80 °C, desolvation temperature 150 °C, cone gas flow rate 60 L/h, desolvation gas flow rate 600 L/h, and nebulizer pressure 6.0 bar. The instrument was calibrated before acquisition using NaI as a reference. UV−vis absorption spectra were recorded on an Agilent 8453 UV−visible Spectroscopy System with the bundled software. Photoluminescence samples were prepared in a standard 1 cm path length quartz cell.

Synthesis of S1. 1,3,5-tribromobenzene (3 g, 9.53 mmol, 1 equiv) and (3-acetylphenyl)boronic acid (7.03 g, 42.88 mmol, 4.5 equiv) in a 250 mL flask were evacuated and flushed with N_2 three times. 40 mL of dioxane and 15 mL of water with dissolved K_2CO_3 (5.27 g, 38.12 mmol, 4 equiv) were added to the flask. The mixture was then degassed by N_2 flushing for 1 h, followed by the addition of tetrakis(triphenylphosphine)palladium(0) (550 mg, 0.476 mmol, 0.05 equiv). The mixture was then heated at 100 °C for 24 h. After the mixture was cooled to ambient temperature, it was evaporated under reduced pressure to obtain the dried solid. The solid was then dissolved in DCM and filtered through Celite. The filtrate was then evaporated and purified by column chromatography (SiO_2, DCM/MeOH, 100:1) to obtain a purified solid and subsequently recrystallized in ACN to obtain a white solid (3.1 g, 7.17 mmol, 75% yield). ^1H NMR (600 MHz, $CDCl_3$): δ 8.28 (s, 3H), 8.00 (d, J = 6.3 Hz, 3H), 7.91 (d, J = 6.3 Hz, 3H), 7.84 (s, 3H), 7.61 (t, J = 7.7 Hz, 3H), 2.69 (s, 9H). ^{13}C NMR (151 MHz, $CDCl_3$): δ 198.05, 141.84, 141.25, 137.78, 132.04, 129.28, 127.83, 127.04, 125.72, 26.87. HRMS (ESI$^+$) $[M + Na]^+$: 455.1629, $[2M + Na]^+$: 887.3352.

Synthesis of HL^{meta}. S1 (300 mg, 0.69 mmol, 1 equiv) was added into a 100 mL two-necked flask, the flask was then vacuum-purged and flushed with nitrogen three times, dry THF (25 mL) was added, and the reaction mixture was cooled to −78 °C by a liquid nitrogen-acetone bath. The reaction mixture was stirred for 15 min and followed by the addition of LiHMDS (1 M in THF, 6.94 mL, 6.94 mmol, 10 equiv) and stirred for a further 30 min. Ethyl heptafluorobutrate (1.20 mL, 6.94 mmol, 10 equiv) was added, the bath was removed, and the reaction mixture was allowed to slowly warm to room temperature. After 4 h, the reaction mixture was heated to 50 °C and stirred for 8 h. Afterward, the reaction was complete. The mixture was evaporated to oil, MeOH (20 mL) was added to dilute the oil, 1 N HCl was added to precipitate until the mixture pH at 2−4, and water was added to the mixture and filtered to obtain a yellow solid. (510 mg, 0.5 mmol, 72% yield). ^1H NMR (600 MHz, $CDCl_3$): δ 8.26 (d, J = 2.3 Hz, 3H), 8.00 (d, J = 7.8 Hz, 3H), 7.96 (d, J = 7.7 Hz, 3H), 7.84 (d, J = 1.7 Hz, 3H), 7.68 (t, J = 7.7 Hz, 3H), 6.70 (s, 3H). ^{13}C NMR (151 MHz, $CDCl_3$): δ 185.32, 179.40, 179.22, 179.05, 141.73, 133.61, 133.14, 133.10, 129.78, 129.73, 127.10, 126.55, 126.03, 118.49, 116.59, 111.08, 109.54, 109.33, 109.12, 94.20. ^{19}F NMR (565 MHz, $CDCl_3$): δ −80.49 (t, J = 9.0 Hz), −121.58 (q, J = 8.8 Hz), −126.75. HRMS (ESI$^-$): $[S2 - H]^-$: 1019.1150.

Synthesis of S2. 1,3,5-tribromobenzene (1.63 g, 5.18 mmol, 1 equiv) and (4-acetylphenyl)boronic acid (3.4 g, 20.71 mmol, 4 equiv) in a 250 mL flask were evacuated and flushed with N_2 three times. 40 mL of dioxane and 15 mL of water with dissolved K_2CO_3 (3.58 g, 25.89 mmol, 5 equiv) were added to the flask. The mixture was then degassed by N_2 flushing for 1 h, followed by the addition of tetrakis(triphenylphosphine)palladium(0) (300 mg, 0.258 mmol, 0.05 equiv). The mixture was then heated at 100 °C for 24 h. The mixture was cooled to ambient temperature and evaporated under reduced pressure to obtain the dried solid. The solid was then dissolved in DCM and filtered through Celite. The filtrate was then evaporated and purified by column chromatography (SiO_2, DCM/MeOH, 100:1) to obtain a white solid and subsequently recrystallized in ACN to obtain a white needle solid (1.8 g, 4.16 mmol, 80% yield). ^1H NMR (600 MHz, $CDCl_3$): δ 8.10 (d, J = 8.1 Hz, 6H), 7.87 (s, 3H), 7.80 (d, J = 8.1 Hz, 6H), 2.67 (s, 9H). ^{13}C NMR (151 MHz, $CDCl_3$): δ 197.71, 145.07, 141.58, 136.37, 129.11, 127.52, 126.13, 26.76. HRMS (ESI$^+$): $[M + H]^+$: 433.1807, $[2M + Na]^+$: 887.3368.

Synthesis of HL^{para}. S2 (382 mg, 0.88 mmol, 1 equiv) was added into a 100 mL two-necked flask, the flask was then vacuum-purged and flushed with nitrogen three times, dry THF (25 mL) was added, the reaction mixture was cooled to −78 °C by a liquid nitrogen-acetone bath, and the reaction mixture was stirred for 15 min,

https://doi.org/10.1021/acs.inorgchem.5c02534
Inorg. Chem. 2025, 64, 20927−20938

followed by the addition of LiHMDS (1 M in THF, 7.95 mL, 7.95 mmol, 9 equiv), and stirred for a further 30 min. Ethyl heptafluorobutrate (1.37 mL, 7.95 mmol, 9 equiv) was added, the bath was removed, and the reaction mixture was allowed to slowly warm to room temperature. After 4 h, the reaction mixture was heated to 50 °C and stirred for 8 h. Afterward, the mixture was evaporated to oil, MeOH (20 mL) was added to dilute the oil, 1 N HCl was added to precipitate until the mixture pH at 2−4, and water was added to the mixture and filtered to obtain a yellow solid (0.86 g, 0.84 mmol, 95%). ^{1}H NMR (600 MHz, $CDCl_3$): δ 15.34 (s, 3H), 8.11 (d, J = 8.0 Hz, 6H), 7.91 (s, 3H), 7.86 (d, J = 8.0 Hz, 6H), 6.69 (s, 3H). ^{13}C NMR (151 MHz, $CDCl_3$): δ 184.67, 179.55, 179.38, 179.20, 145.97, 141.45, 132.15, 128.51, 127.93, 126.41, 93.92. ^{19}F NMR (565 MHz, $CDCl_3$): δ −80.47 (t, J = 8.8 Hz), −121.59 (q, J = 9.0 Hz), −126.76. HRMS (ESI^-): $[M - H]^-$: 1019.1010, $[M - 2H]^{2-}$: 509.0478.

General Synthesis of $Eu_3(L^{meta})_3(L^{R/S})_3$ and $Eu_4(L^{para})_4(L^{R/S})_4$ $L^{R/S}$ = (*R*)- or (*S*)-BINAPO. Diketone ligand L^{para}/L^{meta} (25 mg, 24.5 μmol, 1 equiv) and methanol (10 mL) were added to a 25 mL flask, followed by the addition of triethylamine (10.24 μL, 73.5 μmol, 3 equiv). After all the suspension dissolved, (*S*)/(*R*)-BINAPO (24.5 μmol, 1 equiv) dissolved in DCM (1 mL) was added to the reaction mixture. After stirring for 5 min, $LnCl_3(H_2O)_6$ (8.98 mg, 24.5 μmol, 1 equiv) dissolved in MeOH (1 mL) was added to the reaction mixture dropwise under vigorous stirring. Then, the reaction mixture was added with DCM (10 mL) and heated to reflux temperature for 12 h. The resulting mixture was then evaporated to dryness and washed by the addition of water to remove the triethylamine hydrochloride salt. The solid was then isolated and dried under vacuum to obtain the solid. However, the ^{1}H NMR spectra were difficult to assign due to the paramagnetic nature of Eu(III). Mass spectrum analyses confirm the successful formation of the corresponding complexes.

$Eu_3(L^{meta})_3(L^R)_3$ (90% Yield). See the ^{1}H NMR spectrum in the Supporting Information. ^{19}F NMR (565 MHz, $CDCl_3$): δ − 80.20 (s, 9F), −80.47 (s, 9F), −83.35 (s, 9F), −118.97 (d, J = 271.4 Hz, 3F), −120.29 (d, J = 268.5 Hz, 3F), −122.00 (d, J = 270.8 Hz, 3F), −123.24 − − 126.91 (m, 15F), −129.14 (d, J = 266.1 Hz, 3F), −129.27 (d, J = 266.7 Hz, 3F), −130.26 − − 131.99 (m, 6F). ^{31}P NMR (243 MHz, $CDCl_3$): δ − 43.75 (s, 3P), −48.37 (s, 3P). HRMS (ESI^+): $[M + 2Na]^{2+}$: 2759.3164, $[M - L^R + 2Na]^{2+}$: 2431.7275, $[M - 2L^R + Na]^+$: 4186.2612, $[M - 3L^R + Na]^+$: 3531.0505.

$Eu_3(L^{meta})_3(L^S)_3$ (90% Yield). See ^{1}H NMR spectrum in the Supporting Information. ^{19}F NMR (565 MHz, $CDCl_3$): δ −80.21 (s, 9F), −80.53 (s, 9F), −83.32 (s, 9F), −119.25 (d, J = 272.0 Hz, 3F), −120.25 (d, J = 267.3 Hz, 3F), −122.15 (d, J = 272.5 Hz, 3F), −123.21 − −126.82 (m, 15F), −129.15 (d, J = 265.6 Hz, 3F), −129.20 (d, J = 272.9 Hz, 3F), −130.38 − −132.21 (m, 6F). ^{31}P NMR (243 MHz, $CDCl_3$): δ −43.68 (s, 3P), −48.39 (s, 3P). HRMS (ESI^+): $[M + 2Na]^{2+}$: 2759.3164, $[M - L^S + 2Na]^{2+}$: 2431.7275, $[M - 2L^R + Na]^+$: 4186.2691, $[M - 2L^S + 2Na]^{2+}$: 2104.6230, $[M - 3L^R + Na]^+$: 3531.0505.

$Eu_4(L^{para})_4(L^R)_4$ (95% Yield). See ^{1}H NMR spectrum in the Supporting Information. ^{19}F NMR (376 MHz, $CDCl_3$): δ −80.80 (s, 36F), −122.65 (s, 24F), −126.72 (s, 24F). ^{31}P NMR (162 MHz, $CDCl_3$): δ − 73.51 (s, 8P). HRMS (ESI^+): $[M + 2Na]^{2+}$: 3671.3606, $[M - L^R + 2Na]^{2+}$: 3344.2769, $[M - 2L^R + 2Na]^{2+}$: 3016.6807, $[M - 3L^R + 2Na]^{2+}$: 2689.5786.

$Eu_4(L^{para})_4(L^S)_4$ (95% yield). See ^{1}H NMR spectrum in the Supporting Information. ^{19}F NMR (376 MHz, $CDCl_3$): δ −80.79 (s, 36F), −122.77 (s, 24F), −126.77 (s, 24F). ^{31}P NMR (243 MHz, $CDCl_3$): δ −74.49 (s, 8P). HRMS (ESI^+): $[M + 2Na]^{2+}$: 3671.4167, $[M - L^R + 2Na]^{2+}$: 3344.3472, $[M - 2L^R + 2Na]^{2+}$: 3016.7148.

$Gd_3(L^{meta})_3(L^S)_3$ (90% Yield). HRMS (ESI^+): $[M + 2Na]^{2+}$: 2767.2520.

$Gd_4(L^{para})_4(L^S)_4$ (90% Yield). HRMS (ESI^+): $[M + 2Na]^{2+}$: 3681.8674, $[M - L^R + 2Na]^{2+}$: 3354.2798, $[M - 2L^R + 2Na]^{2+}$: 3027.1660, $[M - 3L^R + 2Na]^{2+}$: 2699.5930.

Photophysical Studies. Emission and excitation spectra were recorded using an Edinburgh Instrument FLSP920 spectrophotometer with an Xe900 xenon lamp. The sample is prepared at 0.1 Abs of the excitation wavelength in a standard 1 cm path length quartz cell. Emission and excitation spectra were recorded and corrected with the correction file from the bundled F900 software. The emission lifetime of Eu(III) compound was measured using the Edinburgh instrument mini-τ with MCS, with the bundled F980 software, 340 nm UV VPLED as an excitation source. The quantum yields of the europium complexes were determined by the absolute method using the integrating sphere accessory configured for the direct excitation method for the Edinburgh Instrument FLSP920 spectrophotometer at ambient conditions. The absolute quantum yield of the sample was calculated using the following equation

$$\Phi_{tot} = \frac{\int Em_{Sample} - \int Em_{Blank}}{\int Sc_{Blank} - \int Sc_{Sample}} \quad (1)$$

where Em is the emission range and Sc is the scatter region recorded using the integrating sphere. The reported quantum yields were averaged over three independent measurements, and all measured quantum yields are within 5% error. Intrinsic quantum yield (Φ_{Eu}^{Eu}) and the sensitization efficiency (η_{sens}) were calculated from the following equations[101]

$$\Phi_{tot} = \eta_{sens}\Phi_{Eu}^{Eu} \quad (2)$$

$$\Phi_{Eu}^{Eu} = \frac{\tau_{obs}}{\tau^{rad}} \quad (3)$$

$$\frac{1}{\tau^{rad}} = A_{MD,0}\cdot n^3\left(\frac{I_{tot}}{I_{MD}}\right) \quad (4)$$

where $1/\tau^{rad}$ is the rate of the spontaneous emission and τ_{obs} is the observed emission rate. $A_{MD,0}$ is the Einstein coefficient of the Eu (III) MD transition in vacuo as a constant of 14.65 s^{-1}, n is the refractive index of the solvent used, and I_{tot} and I_{MD} are the integrated emission intensity of all Eu (III) $^5D_0$ to ^7F_J transitions and solely the $^5D_0$ to $^7F_1$ transition, respectively.

The emission spectra of Gd complexes were recorded in the Edinburgh Instrument FLSP920 spectrophotometer with a Xe900 xenon lamp, room temperature measurement was conducted in a standard 1 cm path length quartz cell, and low temperature measurement was conducted using a Dewar sample holder with the temperature maintained at 77 K. The sample was dissolved in a 1:4 methanol: ethanol mixture to maintain the transparency. The emission lifetime of Gd complexes was recorded in an FLSP920 spectrophotometer with an mF920 μs flash lamp for low temperature measurements and an Edinburgh Instrument mini-τ in time-correlated single photon counting mode with a 340 nm EPLED picosecond laser for room temperature measurements. The recorded data are fitted with the bundled F980 software, accounting for the instrument response function for fast photoluminescence lifetime. All the spectroscopic measurements were conducted in triplicate, and the data were processed using Origin 2024b.

Chiroptical Studies. CD spectra were recorded on a JASCO J-1500 Circular Dichroism Spectrometer with the bundled software. CPL spectra were recorded on a JASCO CPL-300 CPL Spectrometer with the bundled software.

X-ray Crystal Structure. Data for $[Eu_3(L^{meta})_3(L^S)_3]$ were collected on a Bruker D8 Venture Diffractometer System with a microfocus Mo−Kα X-ray source and a PHOTON III detector. The crystal was coated in the inert Parabar 10312 cryoprotectant, after which it was placed under a constant stream of nitrogen at 100(2) K. A full sphere of data were collected using a combination of phi and omega scans, and out of a total of 958325 reflections collected, 67131were unique (Rint = 0.0533). Multiscan absorption correction was applied by the SADABS program, and the SAINT program was utilized for the integration of the diffraction profile. The structure was solved by the direct method and was refined by a full-matrix least-squares treatment on F^2 using the SHELXLE program system. The structure was displayed with "VESTA ver. 3.90.5a" for the polyhedral figure,[102] "Mercury ver. 2024.3.1" for the others.[103] The fluoroalkyl chains all exhibited a varying level of disorder, however, with low level

https://doi.org/10.1021/acs.inorgchem.5c02534
Inorg. Chem. 2025, 64, 20927−20938

residual electron density (ca. < 1.5 eÅ^{-3}) distributed in a very diffused manner, it was insufficient in modeling the disorder. While these disordered groups were all allowed to refine freely initially, several of these groups required their position and displacement parameters to be locked in order to maintain sensible geometry and allow for convergence during refinement. Similarly, residual electron density in the large solvent accessible void was too diffuse and incoherent for modeling of any solvent molecule. The SQUEEZE/PLATON was considered unnecessary as residual electron density was small enough, and the procedure was unlikely to significantly alter the refinement. All atoms were otherwise refined anisotropically, and hydrogen atoms were refined on a suitable riding model. The final *R*-values were: R_1 = 0.0714 [$I > 2\,s(I)$] and wR_2 = 0.2049 (all data), with restrained GooF on F^2 = 1.116. CCDC of $Eu_3(\mathbf{L}^{meta})_3(L^S)_3$: 2450289

■ ASSOCIATED CONTENT

Supporting Information

The Supporting Information is available free of charge at https://pubs.acs.org/doi/10.1021/acs.inorgchem.5c02534.

Experimental methods for this work, single crystal X-ray diffraction, ^{1}H, ^{19}F, ^{31}P, ^{13}C NMR, 2D NMR, ESI-MS, UV−vis absorption, excitation and emission spectra, emission decay profiles, g_{lum} profile, and tables for the crystal refinement results (PDF)

Accession Codes

Deposition Number 2450289 contains the supplementary crystallographic data for this paper. These data can be obtained free of charge via the joint Cambridge Crystallographic Data Centre (CCDC).

■ AUTHOR INFORMATION

Corresponding Author

Ga-Lai Law − *Department of Applied Biology and Chemical Technology, The Hong Kong Polytechnic University, Kowloon 999077 Hong Kong, Special Administrative Region of China;* orcid.org/0000-0002-2192-6887; Email: ga-lai.law@polyu.edu.hk

Authors

Chi-Tung Yeung − *Department of Applied Biology and Chemical Technology, The Hong Kong Polytechnic University, Kowloon 999077 Hong Kong, Special Administrative Region of China*

Sai-Kit Cheung − *Department of Applied Biology and Chemical Technology, The Hong Kong Polytechnic University, Kowloon 999077 Hong Kong, Special Administrative Region of China*

Ho-Yin Wong − *Department of Applied Biology and Chemical Technology, The Hong Kong Polytechnic University, Kowloon 999077 Hong Kong, Special Administrative Region of China*

Wesley Ting Kwok Chan − *Department of Applied Biology and Chemical Technology, The Hong Kong Polytechnic University, Kowloon 999077 Hong Kong, Special Administrative Region of China*

Junhui Zhang − *Department of Applied Biology and Chemical Technology, The Hong Kong Polytechnic University, Kowloon 999077 Hong Kong, Special Administrative Region of China*

Chun-Ming Chan − *Department of Applied Biology and Chemical Technology, The Hong Kong Polytechnic University, Kowloon 999077 Hong Kong, Special Administrative Region of China;* orcid.org/0000-0003-3859-8477

Wai-Lun Man − *Department of Chemistry, Hong Kong Baptist University, Kowloon 999077 Hong Kong, Special Administrative Region of China;* orcid.org/0000-0001-5005-032X

Complete contact information is available at: https://pubs.acs.org/10.1021/acs.inorgchem.5c02534

Author Contributions

Ga-Lai Law conceived and supervised the project. Chi-Tung Yeung acquired the crystals of the compound and prepared the manuscript. Sai-Kit Cheung performed the synthesis of the compounds and the majority of the characterization. Ho-Yin Wong performed a feasibility investigation of the project and the preliminary synthetic work. Wesley Ting Kwok Chan solved the crystal structure. Junhui Zhang conducted the CPL measurements and supervised the photophysical measurements. Chun-Ming Chan assisted with some of the NMR experiments. Wai-Lun Man provided the X-ray machinery and assisted with the preliminary data collection of the crystal structure.

Notes

The authors declare no competing financial interest.

■ ACKNOWLEDGMENTS

We gratefully acknowledge the funding from The Hong Kong Polytechnic University, [University Research Facility for Chemical and Environmental Analysis (UCEA) and University Research Facility in Life Sciences (ULS)]. We acknowledge Ziwei Xu for the cover artwork. We thank Kenneth Siu-Cheong Yan for processing 2D NMR.

■ REFERENCES

(1) Muller, G. Luminescent Chiral Lanthanide(III) Complexes as Potential Molecular Probes. *Dalton Trans.* **2009**, *44*, 9692.

(2) Huo, S.; Duan, P.; Jiao, T.; Peng, Q.; Liu, M. Self-Assembled Luminescent Quantum Dots To Generate Full-Color and White Circularly Polarized Light. *Angew. Chem., Int. Ed.* **2017**, *56* (40), 12174−12178.

(3) Feringa, B. L. In Control of Motion: From Molecular Switches to Molecular Motors. *Acc. Chem. Res.* **2001**, *34* (6), 504−513.

(4) Huck, N. P. M.; Jager, W. F.; de Lange, B.; Feringa, B. L. Dynamic Control and Amplification of Molecular Chirality by Circular Polarized Light. *Science* **1996**, *273* (5282), 1686−1688.

(5) Wang, C.; Fei, H.; Qiu, Y.; Yang, Y.; Wei, Z.; Tian, Y.; Chen, Y.; Zhao, Y. Photoinduced Birefringence and Reversible Optical Storage in Liquid-Crystalline Azobenzene Side-Chain Polymers. *Appl. Phys. Lett.* **1999**, *74* (1), 19−21.

(6) Novikova, T.; Pierangelo, A.; De Martino, A.; Benali, A.; Validire, P. Polarimetric Imaging for Cancer Diagnosis and Staging. *Opt. Photonics News* **2012**, *23* (10), 26.

(7) Zhang, J.; Dai, L.; Webster, A. M.; Chan, W. T. K.; Mackenzie, L. E.; Pal, R.; Cobb, S. L.; Law, G.-L. Unusual Magnetic Field Responsive Circularly Polarized Luminescence Probes with Highly Emissive Chiral Europium(III) Complexes. *Angew. Chem., Int. Ed.* **2021**, *60* (2), 1004−1010.

(8) Chang, V. Y.; Calvinho, K. U. D.; Tovar, R. C.; Johnson, V. A.; Straus, D. A.; Muller, G. Photophysical and Chiroptical Properties of the Enantiomers of *N,N′*-Bis(1-phenylpropyl)-2,6-pyridinecarboxamide and Their Chiral 9-Coordinate Ln $^{3+}$ Complexes. *Eur. J. Inorg. Chem.* **2020**, *2020* (40), 3815−3828.

(9) Ruggieri, S.; Willis, O. G.; Mizzoni, S.; Cavalli, E.; Sanadar, M.; Melchior, A.; Zinna, F.; Di Bari, L.; Bisag, G. D.; Fochi, M.; Bernardi, L.; Piccinelli, F. Near Infrared−Circularly Polarized Luminescence/Circular Dichroism Active Yb(III) Complexes Bearing Both Central and Axial Chirality. *Inorg. Chem.* **2025**, *64* (11), 5505−5512.

(10) Barry, D. E.; Kitchen, J. A.; Mercs, L.; Peacock, R. D.; Albrecht, M.; Gunnlaugsson, T. Chiral Luminescent Lanthanide Complexes

Possessing Strong (Samarium, Sm^{III}) Circularly Polarised Luminescence (CPL), and Their Self-Assembly into Langmuir−Blodgett Films. *Dalton Trans.* **2019**, *48* (30), 11317−11325.
(11) Li, W.; Yin, S.; Song, Z.; Yan, P.; Zhou, Y.; Gao, T.; Li, H. Solvent and Counterion Cooperatively Induced Inversion of the Stereocenter Δ/Λ and CPL in a Mononuclear Eu(III) Complex. *Inorg. Chem. Front.* **2025**, *12* (3), 1176−1186.
(12) Shirai, S.; Muratsugu, S.; Matsui, H.; Harada, K.; Ehara, M.; Nakai, H.; Tada, M. Circularly Polarized Luminescence Induction on a Tb(III) Complex with a Tris(*o-Tert*-Butylaryloxide)-Functionalized 1,4,7-Triazacyclononane Ligand Coordinating Chiral 1-Phenylethylamine. *Chem. Commun.* **2024**, *60* (96), 14180−14183.
(13) Willis, O. G.; Petri, F.; De Rosa, D. F.; Mandoli, A.; Pal, R.; Zinna, F.; Di Bari, L. Two-Photon Circularly Polarized Luminescence of Chiral Eu Complexes. *J. Am. Chem. Soc.* **2023**, *145* (46), 25170−25176.
(14) MacKenzie, L. E.; Pal, R. Circularly Polarized Lanthanide Luminescence for Advanced Security Inks. *Nat. Rev. Chem.* **2021**, *5* (2), 109−124.
(15) Parker, D.; Fradgley, J. D.; Wong, K.-L. The Design of Responsive Luminescent Lanthanide Probes and Sensors. *Chem. Soc. Rev.* **2021**, *50* (14), 8193−8213.
(16) Willis, O. G.; Zinna, F.; Di Bari, L. NIR-Circularly Polarized Luminescence from Chiral Complexes of Lanthanides and d-Metals. *Angew. Chem., Int. Ed.* **2023**, *62*, No. e202302358.
(17) Bradberry, S. J.; Savyasachi, A. J.; Martinez-Calvo, M.; Gunnlaugsson, T. Development of responsive visibly and NIR luminescent and supramolecular coordination self-assemblies using lanthanide ion directed synthesis. *Coord. Chem. Rev.* **2014**, *273*−*274*, 226−241.
(18) Mattei, C. A.; Dhbaibi, K.; Lefeuvre, B.; Dorcet, V.; Argouarch, G.; Cador, O.; Le Guennic, B.; Maury, O.; Lalli, C.; Guy, S.; Bensalah-Ledoux, A.; Riobé, F.; Baguenard, B.; Pointillart, F. Circularly polarized luminescence of Eu(III) complexes with chiral 1,10-bi-2-naphthol-derived bisphosphate ligands. *Chirality* **2022**, *34*, 34−47.
(19) Li, Y.; Yagi, A.; Itami, K. Synthesis of Highly Twisted, Nonplanar Aromatic Macrocycles Enabled by an Axially Chiral 4,5-Diphenylphenanthrene Building Block. *J. Am. Chem. Soc.* **2020**, *142* (6), 3246−3253.
(20) Takaishi, K.; Iwachido, K.; Ema, T. Solvent-Induced Sign Inversion of Circularly Polarized Luminescence: Control of Excimer Chirality by Hydrogen Bonding. *J. Am. Chem. Soc.* **2020**, *142* (4), 1774−1779.
(21) Lee, S.; Kim, K. Y.; Jung, S. H.; Lee, J. H.; Yamada, M.; Sethy, R.; Kawai, T.; Jung, J. H. Finely Controlled Circularly Polarized Luminescence of a Mechano-Responsive Supramolecular Polymer. *Angew. Chem., Int. Ed.* **2019**, *58* (52), 18878−18882.
(22) Lunkley, J. L.; Shirotani, D.; Yamanari, K.; Kaizaki, S.; Muller, G. Extraordinary Circularly Polarized Luminescence Activity Exhibited by Cesium Tetrakis(3-Heptafluoro-Butylryl-(+)-Camphorato) Eu(III) Complexes in EtOH and $CHCl_3$ Solutions. *J. Am. Chem. Soc.* **2008**, *130* (42), 13814−13815.
(23) Tsurui, M.; Takizawa, R.; Kitagawa, Y.; Wang, M.; Kobayashi, M.; Taketsugu, T.; Hasegawa, Y. Chiral Tetrakis Eu(III) Complexes with Ammonium Cations for Improved Circularly Polarized Luminescence. *Angew. Chem., Int. Ed.* **2024**, *63* (34), No. e202405584.
(24) Stang, P. J.; Olenyuk, B. Self-Assembly, Symmetry, and Molecular Architecture: Coordination as the Motif in the Rational Design of Supramolecular Metallacyclic Polygons and Polyhedra. *Acc. Chem. Res.* **1997**, *30* (12), 502−518.
(25) Smulders, M. M. J.; Riddell, I. A.; Browne, C.; Nitschke, J. R. Building on Architectural Principles for Three-Dimensional Metallosupramolecular Construction. *Chem. Soc. Rev.* **2013**, *42* (4), 1728−1754.
(26) Holliday, B. J.; Mirkin, C. A. Strategies for the Construction of Supramolecular Compounds through Coordination Chemistry. *Angew. Chem., Int. Ed. Engl.* **2001**, *40* (11), 2022−2043.
(27) Tesfaye, D.; Linert, W.; Gebrezgiabher, M.; Bayeh, Y.; Elemo, F.; Sani, T.; Kalarikkal, N.; Thomas, M. Iron(II) Mediated Supramolecular Architectures with Schiff Bases and Their Spin-Crossover Properties. *Molecules* **2023**, *28* (3), 1012.
(28) Momeni, B. Z.; Davarzani, N.; Janczak, J.; Ma, N.; Abd-El-Aziz, A. S. Progress in Design and Applications of Supramolecular Assembly of 2,2′:6′,2″-Terpyridine-Based First Row d-Block Elements. *Coord. Chem. Rev.* **2024**, *506*, 215619.
(29) Henwood, A. F.; Hegarty, I. N.; McCarney, E. P.; Lovitt, J. I.; Donohoe, S.; Gunnlaugsson, T. Recent Advances in the Development of the Btp Motif: A Versatile Terdentate Coordination Ligand for Applications in Supramolecular Self-Assembly, Cation and Anion Recognition Chemistries. *Coord. Chem. Rev.* **2021**, *449*, 214206.
(30) Sun, Y.; Chen, C.; Stang, P. J. Soft Materials with Diverse Suprastructures via the Self-Assembly of Metal−Organic Complexes. *Acc. Chem. Res.* **2019**, *52* (3), 802−817.
(31) Saha, S.; Regeni, I.; Clever, G. H. Structure Relationships between Bis-Monodentate Ligands and Coordination Driven Self-Assemblies. *Coord. Chem. Rev.* **2018**, *374*, 1−14.
(32) Saha, M. L.; Yan, X.; Stang, P. J. Photophysical Properties of Organoplatinum(II) Compounds and Derived Self-Assembled Metallacycles and Metallacages: Fluorescence and Its Applications. *Acc. Chem. Res.* **2016**, *49* (11), 2527−2539.
(33) Nishioka, Y.; Yamaguchi, T.; Kawano, M.; Fujita, M. Asymmetric [2 + 2] Olefin Cross Photoaddition in a Self-Assembled Host with Remote Chiral Auxiliaries. *J. Am. Chem. Soc.* **2008**, *130* (26), 8160−8161.
(34) Hastings, C. J.; Pluth, M. D.; Bergman, R. G.; Raymond, K. N. Enzymelike Catalysis of the Nazarov Cyclization by Supramolecular Encapsulation. *J. Am. Chem. Soc.* **2010**, *132* (20), 6938−6940.
(35) Morimoto, M.; Bierschenk, S. M.; Xia, K. T.; Bergman, R. G.; Raymond, K. N.; Toste, F. D. Advances in Supramolecular Host-Mediated Reactivity. *Nat. Catal.* **2020**, *3* (12), 969−984.
(36) Kaphan, D. M.; Levin, M. D.; Bergman, R. G.; Raymond, K. N.; Toste, F. D. A Supramolecular Microenvironment Strategy for Transition Metal Catalysis. *Science* **2015**, *350* (6265), 1235−1238.
(37) Mal, P.; Breiner, B.; Rissanen, K.; Nitschke, J. R. White Phosphorus Is Air-Stable Within a Self-Assembled Tetrahedral Capsule. *Science* **2009**, *324* (5935), 1697−1699.
(38) Ziegler, M.; Brumaghim, J. L.; Raymond, K. N. Stabilization of a Reactive Cationic Species by Supramolecular Encapsulation. *Angew. Chem., Int. Ed.* **2000**, *39* (22), 4119−4121.
(39) Therrien, B.; Süss-Fink, G.; Govindaswamy, P.; Renfrew, A. K.; Dyson, P. J. The "Complex-in-a-Complex" Cations $[(acac)_2M{\subset}Ru_6(p\text{-}iPrC_6H_4Me)_6(tpt)_2(dhbq)_3]^{6+}$: A Trojan Horse for Cancer Cells. *Angew. Chem., Int. Ed.* **2008**, *47* (20), 3773−3776.
(40) Lewis, J. E. M.; Gavey, E. L.; Cameron, S. A.; Crowley, J. D. Stimuli-Responsive Pd_2L_4 Metallosupramolecular Cages: Towards Targeted Cisplatin Drug Delivery. *Chem. Sci.* **2012**, *3* (3), 778−784.
(41) Han, J.; Schmidt, A.; Zhang, T.; Permentier, H.; Groothuis, G. M. M.; Bischoff, R.; Kühn, F. E.; Horvatovich, P.; Casini, A. Bioconjugation Strategies to Couple Supramolecular Exo-Functionalized Palladium Cages to Peptides for Biomedical Applications. *Chem. Commun.* **2017**, *53* (8), 1405−1408.
(42) Lu, Z.; Ronson, T. K.; Nitschke, J. R. Reversible Reduction Drives Anion Ejection and C_{60} Binding within an $Fe^{II}_4L_6$ Cage. *Chem. Sci.* **2020**, *11* (4), 1097−1101.
(43) Han, M.; Michel, R.; He, B.; Chen, Y.; Stalke, D.; John, M.; Clever, G. H. Light-Triggered Guest Uptake and Release by a Photochromic Coordination Cage. *Angew. Chem., Int. Ed.* **2013**, *52* (4), 1319−1323.
(44) Bell, D. J.; Natrajan, L. S.; Riddell, I. A. Design of Lanthanide Based Metal−Organic Polyhedral Cages for Application in Catalysis, Sensing, Separation and Magnetism. *Coord. Chem. Rev.* **2022**, *472*, 214786.
(45) Zhong, Y.; Wu, Z.; Zhang, Y.; Dong, B.; Bai, X. Circularly Polarized Luminescence of Lanthanide Complexes: From Isolated Individuals, Discrete Oligomers, to Hierarchical Assemblies. *InfoMat* **2023**, *5* (3), No. e12392.

https://doi.org/10.1021/acs.inorgchem.5c02534
Inorg. Chem. 2025, 64, 20927−20938

(46) Wong, H.-Y.; Lo, W.-S.; Yim, K.-H.; Law, G.-L. Chirality and Chiroptics of Lanthanide Molecular and Supramolecular Assemblies. *Chem* **2019**, *5* (12), 3058−3095.
(47) Barry, D. E.; Caffrey, D. F.; Gunnlaugsson, T. Lanthanide-Directed Synthesis of Luminescent Self-Assembly Supramolecular Structures and Mechanically Bonded Systems from Acyclic Coordinating Organic Ligands. *Chem. Soc. Rev.* **2016**, *45* (11), 3244−3274.
(48) Dhbaibi, K.; Grasser, M.; Douib, H.; Dorcet, V.; Cador, O.; Vanthuyne, N.; Riobé, F.; Maury, O.; Guy, S.; Bensalah-Ledoux, A.; Baguenard, B.; Rikken, G. L. J. A.; Train, C.; Le Guennic, B.; Atzori, M.; Pointillart, F.; Crassous, J. Multifunctional Helicene-Based Ytterbium Coordination Polymer Displaying Circularly Polarized Luminescence, Slow Magnetic Relaxation and Room Temperature Magneto-Chiral Dichroism. *Angew. Chem., Int. Ed.* **2023**, *62*, No. e202215558.
(49) El Aroussi, B.; Zebret, S.; Besnard, C.; Perrottet, P.; Hamacek, J. Rational Design of a Ternary Supramolecular System: Self-Assembly of Pentanuclear Lanthanide Helicates. *J. Am. Chem. Soc.* **2011**, *133*, 10764−10767.
(50) Souri, N.; Tian, P.; Platas-Iglesias, C.; Wong, K.-L.; Nonat, A.; Charbonniére, L. J. Upconverted Photosensitization of Tb Visible Emission by NIR Yb Excitation in Discrete Supramolecular Heteropolynuclear Complexes. *J. Am. Chem. Soc.* **2017**, *139*, 1456−1459.
(51) Yao, Z.; Zhou, Y.; Gao, T.; Yan, P.; Li, H. Ancillary Ligand Modulated Stereoselective Self-Assembly of Triple-Stranded Eu(III) Helicate Featuring Circularly Polarized Luminescence. *RSC Adv.* **2021**, *11* (18), 10524−10531.
(52) Ma, Q.; Yin, S.; Song, Z.; Gao, T.; Yan, P.; Zhou, Y.; Li, H. Unusual Solvent-Regulated Inversion of a Metal Stereocenter in an Enantiopure Eu_2L_4 Helicate: A New Strategy for CPL Inversion. *Inorg. Chem. Front.* **2024**, *11* (22), 8093−8100.
(53) Bing, T. Y.; Kawai, T.; Yuasa, J. Ligand-to-Ligand Interactions That Direct Formation of D_2-Symmetrical Alternating Circular Helicate. *J. Am. Chem. Soc.* **2018**, *140* (10), 3683−3689.
(54) Yao, Z.; Song, Z.; Yin, S.; Huang, W.; Gao, T.; Yan, P.; Zhou, Y.; Li, H. Dispersion Forces-Driven Hierarchical Assembly of Protein-Like Lanthanide Octamers and Emergent CPL. *Chem.—Eur. J.* **2025**, *31* (8), No. e202403976.
(55) Yan, L.-L.; Tan, C.-H.; Zhang, G.-L.; Zhou, L.-P.; Bünzli, J.-C.; Sun, Q.-F. Stereocontrolled Self-Assembly and Self-Sorting of Luminescent Europium Tetrahedral Cages. *J. Am. Chem. Soc.* **2015**, *137* (26), 8550−8555.
(56) Cai, L.-X.; Yan, L.-L.; Li, S.-C.; Zhou, L.-P.; Sun, Q.-F. Stereocontrolled Self-Assembly and Photochromic Transformation of Lanthanide Supramolecular Helicates. *Dalton Trans.* **2018**, *47* (40), 14204−14210.
(57) Liu, D.; Zhou, Y.; Zhang, Y.; Li, H.; Chen, P.; Sun, W.; Gao, T.; Yan, P. Chiral BINAPO-Controlled Diastereoselective Self-Assembly and Circularly Polarized Luminescence in Triple-Stranded Europium(III) Podates. *Inorg. Chem.* **2018**, *57* (14), 8332−8337.
(58) Yeung, C.-T.; Chan, W. T. K.; Yan, S.-C.; Yu, K.-L.; Yim, K.-H.; Wong, W.-T.; Law, G.-L. Lanthanide Supramolecular Helical Diastereoselective Breaking Induced by Point Chirality: Mixture or P-Helix, M-Helix. *Chem. Commun.* **2015**, *51* (3), 592−595.
(59) Kotova, O.; Comby, S.; Pandurangan, K.; Stomeo, F.; O'Brien, J. E.; Feeney, M.; Peacock, R. D.; McCoy, C. P.; Gunnlaugsson, T. The Effect of the Linker Size in C_2-Symmetrical Chiral Ligands on the Self-Assembly Formation of Luminescent Triple-Stranded Di-Metallic Eu(III) Helicates in Solution. *Dalton Trans.* **2018**, *47* (35), 12308−12317.
(60) Comby, S.; Stomeo, F.; McCoy, C. P.; Gunnlaugsson, T. Formation of Novel Dinuclear Lanthanide Luminescent Samarium(III), Europium(III), and Terbium(III) Triple-Stranded Helicates from a C_2-Symmetrical Pyridine-2,6-dicarboxamide-Based 1,3-Xylenediyl-Linked Ligand in MeCN. *Helv. Chim. Acta* **2009**, *92* (11), 2461−2473.
(61) Zhou, Y.; Yao, Y.; Cheng, Z.; Gao, T.; Li, H.; Yan, P. Point Chirality Controlled Diastereoselective Self-Assembly and Circularly Polarized Luminescence in Quadruple-Stranded Europium(III) Helicates. *Inorg. Chem.* **2020**, *59* (17), 12850−12857.
(62) Hegarty, I. N.; Barry, D. E.; Byrne, J. P.; Kotova, O.; Gunnlaugsson, T. Formation of Lanthanide Luminescent Di-Metallic Helicates in Solution Using a Bis-Tridentate (1,2,3-Triazol-4-yl)-Picolinamide (Tzpa) Ligand. *Chem. Commun.* **2023**, *59* (40), 6044−6047.
(63) Stomeo, F.; Lincheneau, C.; Leonard, J. P.; O'Brien, J. E.; Peacock, R. D.; McCoy, C. P.; Gunnlaugsson, T. Metal-Directed Synthesis of Enantiomerially Pure Dimetallic Lanthanide Luminescent Triple-Stranded Helicates. *J. Am. Chem. Soc.* **2009**, *131* (28), 9636−9637.
(64) Tan, Y. B.; Okayasu, Y.; Katao, S.; Nishikawa, Y.; Asanoma, F.; Yamada, M.; Yuasa, J.; Kawai, T. Visible Circularly Polarized Luminescence of Octanuclear Circular Eu(III) Helicate. *J. Am. Chem. Soc.* **2020**, *142* (41), 17653−17661.
(65) Lemonnier, J.-F.; Guénée, L.; Bernardinelli, G.; Vigier, J.-F.; Bocquet, B.; Piguet, C. Planned Failures from the Principle of Maximum Site Occupancy in Lanthanide Helicates. *Inorg. Chem.* **2010**, *49*, 1252−1265.
(66) Terazzi, E.; Guénée, L.; Bocquet, B.; Lemonnier, J.-F.; Favera, N. D.; Piguet, C. A Simple Chemical Tuning of the Effective Concentration: Selection of Single-, Double-, and Triple-Stranded Binuclear Lanthanide Helicates. *Chem.—Eur. J.* **2009**, *15*, 12719−12732.
(67) Aguilà, D.; Barrios, L. A.; Velasco, V.; Roubeau, O.; Repollés, A.; Alonso, P. J.; Sesé, J.; Teat, S. J.; Luis, F.; Aromí, G. Heterodimetallic [LnLn′] Lanthanide Complexes: Toward a Chemical Design of Two-Qubit Molecular Spin Quantum Gates. *J. Am. Chem. Soc.* **2014**, *136*, 14215−14222.
(68) Aguilà, D.; Barrios, L. A.; Velasco, V.; Arnedo, L.; Aliaga-Alcalde, N.; Menelaou, M.; Teat, S. J.; Roubeau, O.; Luis, F.; Aromí, G. Lanthanide Contraction within a Series of Asymmetric Dinuclear [Ln2] Complexes. *Chem.—Eur. J.* **2013**, *19*, 5881−5891.
(69) Albrecht, M.; Osetska, O.; Fröhlich, R.; Bünzli, J.-C. G.; Aebischer, A.; Gumy, F.; Hamacek, J. Highly Efficient Near-IR Emitting Yb/Yb and Yb/Al Helicates. *J. Am. Chem. Soc.* **2007**, *129*, 14178−14179.
(70) Zhou, Y.; Li, H.; Zhu, T.; Gao, T.; Yan, P. A Highly Luminescent Chiral Tetrahedral $Eu_4L_4(L')_4$ Cage: Chirality Induction, Chirality Memory, and Circularly Polarized Luminescence. *J. Am. Chem. Soc.* **2019**, *141* (50), 19634−19643.
(71) Yao, Z.; Gao, T.; Yan, P.; Zhou, Y.; Li, H. Strong Upconverted Circularly Polarized Emission from a Chiral Tetrahedral Yb/Eu Cage. *Dalton Trans.* **2025**, *54* (14), 5731−5738.
(72) Hu, S.-J.; Guo, X.-Q.; Zhou, L.-P.; Yan, D.-N.; Cheng, P.-M.; Cai, L.-X.; Li, X.-Z.; Sun, Q.-F. Guest-Driven Self-Assembly and Chiral Induction of Photofunctional Lanthanide Tetrahedral Cages. *J. Am. Chem. Soc.* **2022**, *144* (9), 4244−4253.
(73) Zhu, Q.-Y.; Zhou, L.-P.; Cai, L.-X.; Hu, S.-J.; Li, X.-Z.; Sun, Q.-F. Stereocontrolled Self-Assembly of Ln(III)−Pt(II) Heterometallic Cages with Temperature-Dependent Luminescence. *Inorg. Chem.* **2022**, *61* (42), 16814−16821.
(74) Yim, K.-H.; Yeung, C.-T.; Probert, M. R.; Chan, W. T. K.; Mackenzie, L. E.; Pal, R.; Wong, W.-T.; Law, G.-L. Helicate-to-Tetrahedron Transformation of Chiral Lanthanide Supramolecular Complexes Induced by Ionic Radii Effect and Linker Length. *Commun. Chem.* **2021**, *4* (1), 116.
(75) Zhao, T.; Zhang, Y.; Wang, G.; Wang, X.; Feng, P.; Zang, S. Amino-Acid-Induced Circularly Polarized Luminescence of Octahedral Lanthanide Cage. *Angew. Chem., Int. Ed.* **2025**, *64* (11), No. e202421426.
(76) Guo, X.-Q.; Zhou, L.-P.; Hu, S.-J.; Sun, Q.-F. Subtle Adjustments for Constructing Multi-Nuclear Luminescent Lanthanide Organic Polyhedra with Triazole-Based Chelates. *Dalton Trans.* **2024**, *53* (10), 4772−4780.
(77) Yim, K.-H.; Yeung, C.-T.; Wong, M. Y.; Probert, M. R.; Law, G.-L. Differentiable Formation of Chiroptical Lanthanide Heterometallic $Ln_nLn'_{4-n}(L_6)$ (N = 0−4) Tetrahedra with C_2 -Symmetrical

https://doi.org/10.1021/acs.inorgchem.5c02534
Inorg. Chem. 2025, 64, 20927−20938

Bis(Tridentate) Ligands. *Chem.—Eur. J.* **2022**, *28* (56), No. e202201655.
(78) Yeung, C.-T.; Yim, K.-H.; Wong, H.-Y.; Pal, R.; Lo, W.-S.; Yan, S.-C.; Yee-Man Wong, M.; Yufit, D.; Smiles, D. E.; McCormick, L. J.; Teat, S. J.; Shuh, D. K.; Wong, W.-T.; Law, G.-L. Chiral Transcription in Self-Assembled Tetrahedral Eu_4L_6 Chiral Cages Displaying Sizable Circularly Polarized Luminescence. *Nat. Commun.* **2017**, *8* (1), 1128.
(79) El Aroussi, B.; Guénée, L.; Pal, P.; Hamacek, J. Lanthanide-Mediated Supramolecular Cages and Host Guest Interactions. *Inorg. Chem.* **2011**, *50*, 8588−8597.
(80) Hamacek, J.; Bernardinelli, G.; Filinchuk, Y. Tetrahedral Assembly with Lanthanides: Toward Discrete Polynuclear Complexes. *Eur. J. Inorg. Chem.* **2008**, *2008*, 3419−3422.
(81) Li, X.-Z.; Zhou, L.-P.; Yan, L.-L.; Yuan, D.-Q.; Lin, C.-S.; Sun, Q.-F. Evolution of Luminescent Supramolecular Lanthanide $M_{2n}L_{3n}$ Complexes from Helicates and Tetrahedra to Cubes. *J. Am. Chem. Soc.* **2017**, *139* (24), 8237−8244.
(82) Li, X.-Z.; Zhou, L.-P.; Hu, S.-J.; Cai, L.-X.; Guo, X.-Q.; Wang, Z.; Sun, Q.-F. Metal Ion Adaptive Self-Assembly of Photoactive Lanthanide-Based Supramolecular Hosts. *Chem. Commun.* **2020**, *56* (32), 4416−4419.
(83) Tan, Y. B.; Yamada, M.; Katao, S.; Nishikawa, Y.; Asanoma, F.; Yuasa, J.; Kawai, T. Self-Assembled Tetranuclear Eu^{III} Complexes with D_2- and C_{2h}-Symmetrical Square Scaffold. *Inorg. Chem.* **2020**, *59* (17), 12867−12875.
(84) Zhu, Q.-Y.; Zhou, L.-P.; Cai, L.-X.; Li, X.-Z.; Zhou, J.; Sun, Q.-F. Chiral Auxiliary and Induced Chiroptical Sensing with 5d/4f Lanthanide−Organic Macrocycles. *Chem. Commun.* **2020**, *56* (19), 2861−2864.
(85) Louis, M.; Tan, Y. B.; Reine, P.; Katao, S.; Nishikawa, Y.; Asanoma, F.; Kawai, T. Conglomerate, Racemate, and Achiral Crystals of Polymetallic Europium(III) Compounds of Bis- or Tris-β-Diketonate Ligands and Circularly Polarized Luminescence Study. *ACS Omega* **2023**, *8* (6), 5722−5730.
(86) Senegas, J.-M.; Koeller, S.; Bernardinelli, G.; Piguet, C. Isolation and Characterization of the First Circular Single-Stranded Polymetallic Lanthanide-Containing Helicate. *Chem. Commun.* **2005**, *17*, 2235−2237.
(87) Han, S.-L.; Yang, J.; Tripathy, D.; Guo, X.-Q.; Hu, S.-J.; Li, X.-Z.; Cai, L.-X.; Zhou, L.-P.; Sun, Q.-F. Self-Assembly of Lanthanide-Covalent Organic Polyhedra: Chameleonic Luminescence and Efficient Catalysis. *Inorg. Chem.* **2020**, *59* (19), 14023−14030.
(88) Sun, Q.-F.; Iwasa, J.; Ogawa, D.; Ishido, Y.; Sato, S.; Ozeki, T.; Sei, Y.; Yamaguchi, K.; Fujita, M. Self-Assembled $M_{24}L_{48}$ Polyhedra and Their Sharp Structural Switch upon Subtle Ligand Variation. *Science* **2010**, *328* (5982), 1144−1147.
(89) Wang, Z.; He, L.; Liu, B.; Zhou, L.-P.; Cai, L.-X.; Hu, S.-J.; Li, X.-Z.; Li, Z.; Chen, T.; Li, X.; Sun, Q.-F. Coordination-Assembled Water-Soluble Anionic Lanthanide Organic Polyhedra for Luminescent Labeling and Magnetic Resonance Imaging. *J. Am. Chem. Soc.* **2020**, *142* (38), 16409−16419.
(90) Hu, S.-J.; Guo, X.-Q.; Zhou, L.-P.; Cai, L.-X.; Sun, Q.-F. Coordination-Assembled Lanthanide-Organic Ln_3L_3 Sandwiches or Ln_4L_4 Tetrahedron: Structural Transformation and Luminescence Modulation. *Chin. J. Chem.* **2019**, *37* (7), 657−662.
(91) Guo, X.-Q.; Zhou, L.-P.; Cai, L.-X.; Sun, Q.-F. Self-Assembled Bright Luminescent Lanthanide-Organic Polyhedra for Ratiometric Temperature Sensing. *Chem.—Eur. J.* **2018**, *24* (27), 6936−6940.
(92) Moore, E. G.; Xu, J.; Jocher, C. J.; Castro-Rodriguez, I.; Raymond, K. N. Highly luminescent lanthanide complexes of 1-hydroxy-2-pyridinones. *Inorg. Chem.* **2008**, *47* (8), 3105−3118.
(93) Wong, H.-Y.; Chan, W. T. K.; Law, G.-L. Triboluminescence of centrosymmetric lanthanide β-diketonate complexes with aggregation-induced emission. *Molecules* **2019**, *24* (4), 662.
(94) Bünzli, J.-C. G.; Eliseeva, S. V. Basics of Lanthanide Photophysics. In *Lanthanide Luminescence: Photophysical, Analytical and Biological Aspects*; Hänninen, P., Härmä, H., Eds.; Springer Berlin Heidelberg, 2011; pp 1−45..
(95) Woods, J. J.; Wacker, J. N.; Peterson, A.; Abergel, R. J.; Ung, G. Improved Energy Transfer in the Sensitization of Americium Enables Observation of Circularly Polarized Luminescence. *Angew. Chem., Int. Ed.* **2024**, *63* (50), No. e202412535.
(96) Xu, H.; Xie, G.; Han, C.; Zhang, Z.; Deng, Z.; Zhao, Y.; Yan, P.; Liu, S. Influence of molecular configuration and functional substituents on excited state energy levels in two naphthyl-based phosphine oxide hosts. *Org. Electron.* **2012**, *13* (9), 1516−1525.
(97) Thor, W.; Kai, H.-Y.; Yeung, Y.-H.; Wu, Y.; Cheung, T.-L.; Tam, L. K. B.; Zhang, Y.; Charbonnière, L. J.; Tanner, P. A.; Wong, K.-L. Unearthing the Real-Time Excited State Dynamics from Antenna to Rare Earth Ions Using Ultrafast Transient Absorption. *JACS Au* **2024**, *4* (10), 3813−3822.
(98) Latva, M.; Takalo, H.; Mukkala, V.-M.; Matachescu, C.; Rodríguez-Ubis, J. C.; Kankare, J. Correlation between the lowest triplet state energy level of the ligand and lanthanide (III) luminescence quantum yield. *J. Lumin.* **1997**, *75* (2), 149−169.
(99) Steemers, F. J.; Verboom, W.; Reinhoudt, D. N.; van der Tol, E. B.; Verhoeven, J. W. New Sensitizer-Modified Calix [4] arenes Enabling Near-UV Excitation of Complexed Luminescent Lanthanide Ions. *J. Am. Chem. Soc.* **1995**, *117* (37), 9408−9414.
(100) Bünzli, J.-C. G. On the design of highly luminescent lanthanide complexes. *Coord. Chem. Rev.* **2015**, *293*, 19−47.
(101) Aebischer, A.; Gumy, F.; Bünzli, J.-C. G. Intrinsic quantum yields and radiative lifetimes of lanthanide tris (dipicolinates). *Phys. Chem. Chem. Phys.* **2009**, *11* (9), 1346−1353.
(102) Momma, K.; Izumi, F. *VESTA 3* for three-dimensional visualization of crystal, volumetric and morphology data. *J. Appl. Crystallogr.* **2011**, *44* (6), 1272−1276.
(103) Macrae, C. F.; Sovago, I.; Cottrell, S. J.; Galek, P. T. A.; McCabe, P.; Pidcock, E.; Platings, M.; Shields, G. P.; Stevens, J. S.; Towler, M.; et al. *Mercury 4.0*: from visualization to analysis, design and prediction. *J. Appl. Crystallogr.* **2020**, *53* (1), 226−235.

https://doi.org/10.1021/acs.inorgchem.5c02534
Inorg. Chem. 2025, 64, 20927−20938